SAND2022-6490J

Understanding the Electrochemical Performance of FeS_2 Conversion Cathodes

David S. Ashby[1,], Jeffrey S. Horner[2], Grace Whang[3], Aliya S. Lapp[1], Scott A. Roberts[2], Bruce Dunn[3], Igor V. Kolesnichenko[2], Timothy N. Lambert[2], and A. Alec Talin[1,*]*

[1]Sandia National Laboratories, Livermore, California 94550, USA.

[2]Sandia National Laboratories, Albuquerque, New Mexico, 87185, USA

[3]Department of Materials Science and Engineering, University of California, Los Angeles, CA 90095, USA.

***Corresponding Authors:** dsashby18@gmail.com, aatalin@sandia.gov

Keywords: Conversion Cathodes, Li-ion Batteries, Loss Mechanism, Polysulfides, Iron Sulfide, Pressure, Kinetics

ABSTRACT

Conversion cathodes represent a viable route to improve rechargeable Li^+ battery energy densities, but poor electrochemical stability and power density has impeded practical implementation. Here, we explore the impact cell fabrication, electrolyte interaction, and current density have on the electrochemical performance of FeS_2/Li cells by deconvoluting the contributions of the various conversion and intercalation reactions to the overall capacity. By varying the slurry composition and applied pressure, we determine that the capacity loss is primarily due to the large volume changes during (de)lithiation, leading to degradation of the conductive matrix. Through application of an external pressure, the loss is minimized by maintaining the conductive matrix. We further determine that polysulfide loss can be minimized by increasing the current density (>C/10), thus reducing the sulfur formation period. Analysis of the kinetics determines that the conversion reactions are rate limiting, specifically the formation of metallic iron at rates above C/8. While focused on FeS_2, our findings on the influence of pressure, electrolyte interaction, and kinetics are broadly applicable to other conversion cathode systems.

TOC GRAPHICS

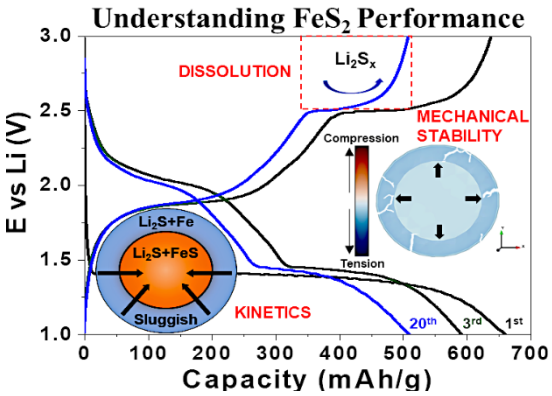

INTRODUCTION

With accelerating demand for electric transportation[1] and grid storage of renewable sources[2], there is an increasing need to design higher energy density batteries. While great gains have been made improving the anode energy density using Li metal or conversion systems such as Si[3] or Li alloys[4,5], strategies to substantially increase the cathode energy density have been less effective, resulting in only incremental gains in lithium-ion batteries (LIB) overall performance. Several conversion-materials (S, FeS_2, FeF_3, CF_x, etc.)[6–8] have attracted interest due to their relatively high potential vs. Li, high theoretical capacity, and success in primary cells; but, to date, they have had mixed success as secondary cells. The poor rechargeability of conversion cathodes has been associated with various material dependent processes, such as dissolution[9–11], particle pulverization[4,12,13], or kinetics[14,15]; however, the manner in which each process affects the electrochemical performance requires further exploration.

Herein, we investigate the cubic FeS_2 system as a prototypical conversion system due to its high theoretical capacity of 894 mAh/g[13] and its success in primary cells.[16] During the first lithiation, FeS_2 irreversibly converts to Li_2S and Fe. Upon Li extraction, the system undergoes a multistep reaction ending with FeS and S as identified in currently-in-review and recent studies.[13] These reactions represent the rechargeable products and progress through a four-electron redox-process involving two conversion reactions (Eq. 1 & 3) bounding an intercalation reaction (Eq. 2).

$$FeS + S + xLi^+ + 2e^- \rightarrow FeS + xLi_2S \text{ (~3-2V, Upper Conversion)} \quad \text{Eq. 1}$$

$$FeS + xLi_2S + yLi^+ + ye^- \rightarrow yLiFeS + xLi_2S \text{ (~2-1.5V, Intercalation)} \quad \text{Eq. 2}$$

$$yLiFeS + xLi_2S + zLi^+ + ze^- \rightarrow Fe + 2Li_2S \text{ (~1.5-1V, Lower Conversion)} \quad \text{Eq. 3}$$

During discharge, the system undergoes an approximately 260% volume expansion,[17] creating stress externally on the conductive matrix and internally on the particle in a manner similar to other conversion electrodes.[3] Measures to mitigate this phenomenon, typically through particle size reduction or matrix engineering,[9,18,19] have been explored with limited success. With an increase in the surface area by using smaller particles, there is an increased chance of detrimental side reactions with the electrolyte,[9,14,15,20] while engineering the matrix, such as through conducting scaffolding, typically leads to a decrease in the active material loading. Particular to the metal sulfide systems, the formation of soluble polysulfide species (PS) at higher voltages leads to significant capacity fading due to PS dissolution and shuttling from the cathode to the anode, which reduces the redox material available at both electrodes.[21] Attempts to reduce the solubility[12,22], trap the sulfur species[23–26], or limit the voltage[27] have had some success, albeit generally at a tradeoff with respect to power and/or energy. Moreover, with conversion reactions requiring the breakage of multiple bonds and long diffusion distances during cycling, conversion materials are typically kinetically limited, lowering the achievable power density. While the kinetics are acknowledged to inhibit access to the entire particle volume[28], it remains unclear which component of the FeS_2 (de)lithiation process is the rate limiting step.

In this study, we deconvolute the impact of cell design, anion dissolution, and reaction kinetics on the performance of FeS_2/Li batteries, consisting of ball-milled, commercially available FeS_2 powder cycled in 1M LiFSI $PYR_{14}TFSI$ electrolyte (ILE). By varying the slurry composition as well as applied pressure during cycling, we determine that for higher weight loading cells (>1 mg/cm^2) applied pressure

is paramount for achieving improved performance, regardless of slurry composition. However, while pressure improves the achievable capacity and stability, significant loss still occurs from PS shuttling where the extent of loss is inversely related to the current density. Analysis of the individual redox reactions at rates ranging from C/40-C/2 indicates that above C/8, the conversion reactions, specifically the slow conversion to metallic Fe leads to notable decreases in the achievable capacity. Our results provide valuable insights into the mechanisms that limit the practical power and energy of FeS_2 conversion cathodes and offer avenues to mitigate these performance limitations, namely the addition of pressure to mitigate pulverization of the slurry matrix and the reduction of polysulfide dissolution at higher rates. While this study focuses on the FeS_2 system, the approach presented herein is applicable as a whole to identify limitations in other conversion cathode systems.

RESULTS AND DISCUSSION

Pressure and Electrical Conductance:

Similar to conversion anodes, the large volumetric changes that accompany (de)lithiation of conversion cathodes can result in pulverization of the slurry matrix, loss of electrical connectivity of the electrode particles[29] and/or exposure of fresh surface to the electrolyte[6] (Figure 1a). We propose that any loss associated with formation of a cathode electrolyte interface is negligible as the conversion cathode voltage window is typically within the stability of most commonly used non-aqueous electrolytes and thus can be ignored.[30] Therefore, we focus on the relationships between cathode slurry composition, cell design, and volume expansion. Strategies to address losses associated with the slurry and particle pulverization in conversion anodes include application of external pressure,[11] decreasing the active material ratio,[22] and lowering the cell loading.[12] In Figure 1b, we explore the effect of each of these factors on FeS_2 electrochemical performance and stability. Similar to what has been reported for conversion anodes,[3] we observe that reduction in the cell loading or increase in the binder/carbon-to-FeS_2 ratio are effective strategies to achieve optimal performance, although a non-negligible capacity loss (~1.5%/cycle) still occurs over the first 5 cycles. More importantly, we find that without significant carbon loadings or stack pressures (~300kPa), applied through a spring (see S.I. Methods), the capacity is low and/or decays rapidly. Analysis of the coulombic efficiency of the cycling in figure 1b supports the improved stability with the addition of pressure (Figure S1). This correlated to an initial efficiency of 85% without pressure versus 91% with pressure before stabilizing to 98% by 5 cycles. These results suggest that, similar to many conversion anodes, scaling up conversion cathodes requires an external or internal pressure to maintain electrode cohesion and retain electrochemical stability as an increased carbon/binder weight percentage is not practical.

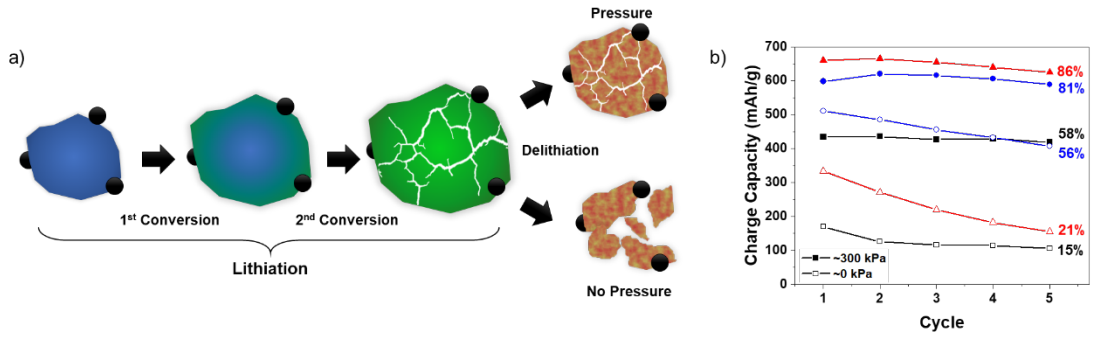

Figure 1: Electrochemical Performance and Cell Design

(a) Volume expansion illustration during (de)lithiation of FeS_2. The color schemes are arbitrarily applied to identify the progression of the reactions.[13] (b) FeS_2/Li cells electrochemical performance cycled at C/10 in ILE with varying cell compositions and pressure: 80 wt% FeS_2/10 wt% C/10 wt% PVDF 2.5 mg/cm^2 (Black), 80 wt% FeS_2/10 wt% C/10 wt% PVDF 1 mg/cm^2 (Red), and 60 wt% FeS_2/20 wt% C/20 wt% PVDF 2.5 mg/cm^2 (Blue). The 5th cycle capacity, normalized to 725 mAh/g, is included.

To better understand how pulverization during (de)lithiation, identified previously,[13,17] leads to capacity loss, we measured the cathode conductance during cycling for different cathode-binder ratios (Figure 2a). An SEM image of the conductance electrode demonstrates the uniform slurry distribution over the gap (Figure 2b). The results illustrate that without significant binder, the conductance decreases significantly upon lithiation (Figure 2c) as the matrix deteriorates from pulverization and electrical isolation of FeS_2 fragments. This suggests that improvement in the cycle stability from addition of pressure (Figure 1b) stems primarily from maintaining a well-connected, coherent matrix throughout cycling. Analysis of the internal stress using a simplified mechanistic model of an individual FeS_2 particle during lithiation indicates that the relatively low applied pressure primarily maintains particle-particle contact (Figure S2). During cycling, high tensile stresses materialize, up to 50 GPa, sufficient for intraphase and, for Li_2S (~40 MPa),[31] interphase fracture leading to particle pulverization as previously identified.[13,17] Incorporating a stack pressure of ~300 kPa, even assuming high local particle-particle stresses, does not have a significant effect on the particle internal stress (Figure 2d); thus, particle cracking should occur regardless of the stack pressure. Scanning electron microscopy (SEM) images of the slurry before and after cycling (Figure S3a,b) support that an applied pressure helps maintain the matrix; yet, interestingly, there is no indication of particle pulverization. Degradation of the FeS_2 morphology though is identified without an applied pressure during cycling (Figure S3c). This material degradation exposes new surface promoting PS shuttling loss in the cell; and thus, a decreasing contribution from the high-voltage conversion reaction involving sulfur, as identified in the capacity deconvolution for the 1 mg/cm^2 cell (red) in Figure 1b (Figure S4). As the stress model is a simple mechanistic system that only addresses the first lithiation, this discrepancy with the SEM data likely stems from changes in the reaction process or dissolution that was not considered. While optimization of the slurry and cell design would address the loss associated with degradation of the conductive matrix, the continued loss even under load in figure 1b suggests that electrode optimization is not the sole solution for stable, rechargeable cycling.

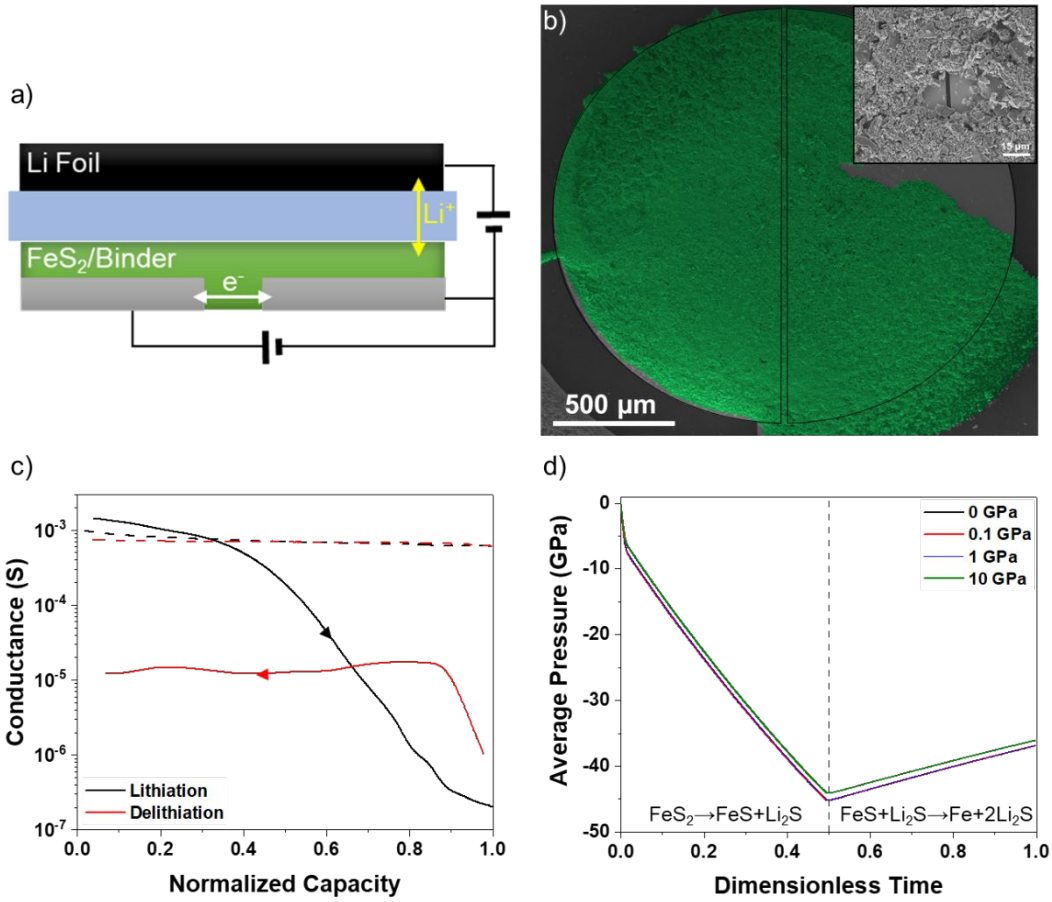

Figure 2: Volume Expansion Cell Degradation

(a) Schematic of FeS_2 conductance measurement. (b) SEM image of conductance electrode consisting of isolated semicircle current collectors separated by a 4 µm gap. The inset shows the slurry distribution over the gap. The slurry is false colored and electrodes are outlined (c) FeS_2 conductance measured across a 4 µm gap during cycling for a slurry composed of 95 wt% FeS_2 (solid lines) or 75 wt% FeS_2 (dashed lines). The remainder consisted of PVDF binder with no carbon. (d) Average internal tension induced during the initial lithiation for arbitrarily sized, unconstrained FeS_2 and anisotropically constrained single particle volume expansion. The constraint was varied between 0.1-10 GPa.

Electrolyte-Cathode Interaction:

Particular to the conversion sulfide systems, PS dissolution presents a notable obstacle for stable cycling with Li-metal cells.[32] While ionic liquids are chosen here due to their low PS solubility,[33] the extent to which PS-shuttling contributes to capacity loss in our experiments needs to be clarified. As mentioned earlier, FeS_2 undergoes an intercalation reaction bounded by two distinct conversion reactions consisting of different sulfides, iron, and sulfur compounds (Figure 3a, Eq. 1-3).[13] In Figure 3b, the contribution of each reaction to the overall capacity is extracted and monitored over 10 cycles at C/40, where the individual components during lithiation, upper conversion (~>2V), intercalation, and lower conversion (~<1.5V), are determined from the dQ/dV (Figure S5). The cell is cycled under ~300 kPa of pressure at a low current density to reduce the influence of volume expansion and kinetics on the

electrochemical performance. This deconvolution reveals that the cathode capacity loss (2.7% per cycle) is primarily associated with the upper conversion reaction (>~2.4V) where the overall capacity contribution due to S_8 formation decreases 1.1% per cycle during charge. This finding confirms that sulfide dissolution persists at low current densities even when a low solubility electrolyte is used.. Moving to an electrolyte with a negligible sulfide solubility[33] has been previously proposed to decrease PS shuttling and improve capacity retention in FeS_2 cell loadings;[22] however, the higher viscosity, pure TFSI electrolyte (1M LiTFSI $PYR_{14}TFSI$) substantially reduced the capacity (95 mAh/g, Figure S6) in our system, likely due to insufficient conduction and wetting. While significant at low currents, this loss, attributable to the upper conversion reaction involving sulfur, decreases as the current density increases (Figure 3c), from approximately 8.4% cell capacity loss over 10 cycles at C/40 to 2% loss over 10 cycles at C/10. We attribute this enhanced cell capacity retention to improved retention of sulfur at higher currents (Figure 3d), which eventually leads to stable cycling at C/8 (-0.3%/cycle) and above. Although there is an appreciable reduction in the achievable capacity at higher rates, our results indicate that operating at higher current densities is a potential route to mitigate PS shuttling effects.

It is unclear what effect the current density has on the long-term life of the cell. Extended cycling at C/10 indicates that the improved stability obtained at higher rates is maintained over 50 cycles with no change in the individual reactions contribution (0.9 mAh/g loss per cycle, Figure S7). To determine the PS effect on aging, the cells cycled at C/10 (final delithiation to 3V) and C/20 (final delithiation to 2V) in Figure 3d were rested for 10 days (Figure S8). We find that both cells maintain their last achievable capacity when recharged after the rest period. This is a surprising result since stopping the C/10 cell after forming sulfur (3V) is expected to lead to significant capacity loss from sulfide dissolution. The maintained capacity for the C/20 cell stopped at 2V correlates with our expectations as sulfur has not been formed. Further work is required to determine if this stability is related to the sulfur species formed at these rates or due to cell relaxation (~2.25 OCV).

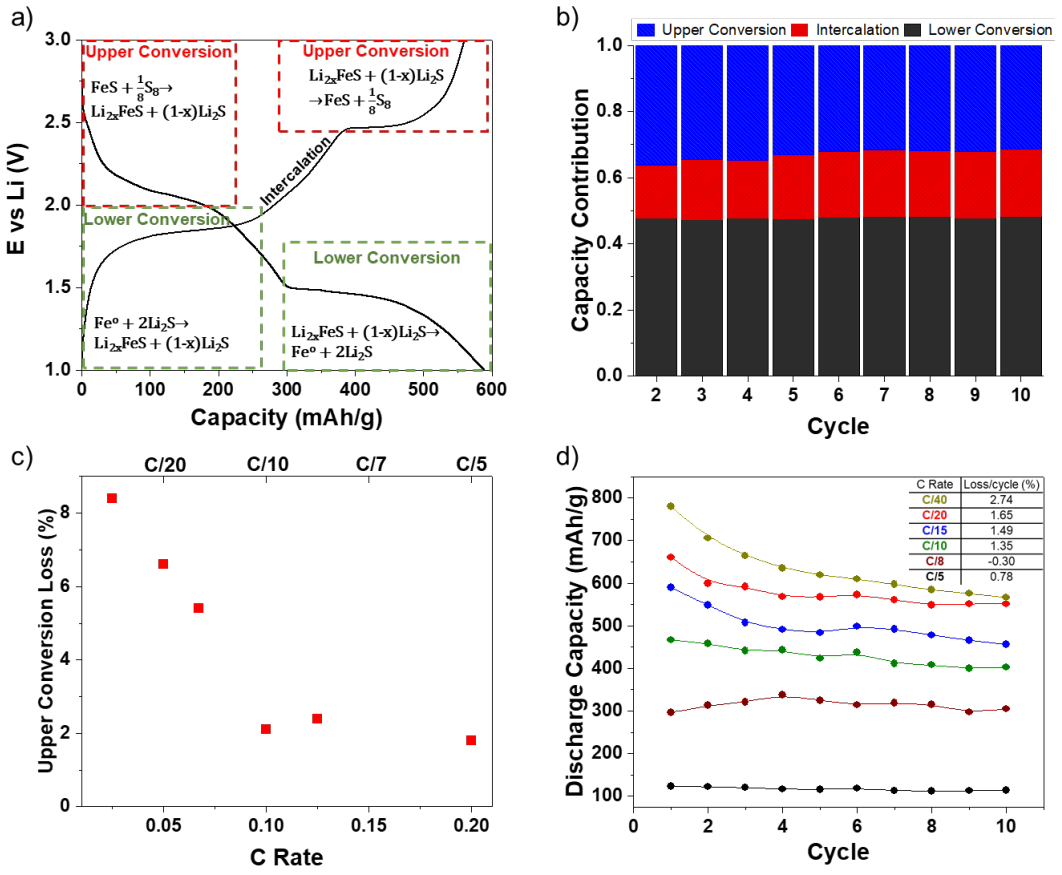

Figure 3: FeS_2 Reactions Loss Mechanism

(a) Reaction mechanisms during cycling of secondary FeS_2/Li cells in ILE. (b) Capacity contribution during discharge of the upper conversion (>~1.9V), intercalation, and lower conversion (~<1.5V) reactions cycled at C/40 over 10 cycles. (c) Overall upper conversion capacity loss over 10 cycles versus cycle rate. (d) Capacity stability over 10 cycles for different cells cycled at rates between C/5-C/40.

FeS_2 Kinetics:

Having established the impact of pressure and polysulfide solubility on the electrochemical performance of conversion FeS_2/Li cells, we now focus on understanding the effect of current density. To limit the impact of cell design and electrolyte interaction with the cathode (e.g. penetration, wetting), a lower weight loading cell (~1.5 mg/cm^2) is analyzed. Cycling of the cell is limited to two cycles for each rate from C/40 to C/2 to minimize PS and matrix loss. The results shown in Figure 4a indicate that cycling our FeS_2 cells at increasing rates decreases the overall capacity, primarily by limiting the contribution of the two conversion reactions. To further illustrate this point, we deconvolute the lithiation capacity contribution of the upper conversion, intercalation, and lower conversion regions (Figure 4b). At rates up to C/8, the relative contributions from the upper and lower conversion reactions dominate but decrease steadily with increasing C-rates. Above C/8, the conversion reactions contribution to the cell capacity significantly decreases due to kinetic limitations, causing the capacity to be dominated by the intercalation reaction. This decrease in the conversion contributions is more pronounced for the low-

voltage reaction suggesting that, while both reactions are sluggish, the conversion involving Fe^0 is the rate limiting step in iron-sulfide systems. This result suggests that micron-size FeS_2 powder (Figure S9) is not suitable for higher power density rechargeable applications, particularly since scaling up and optimizing the cathode composition will only exacerbate the kinetic limitation. Several routes have had success addressing the sluggish kinetics of FeS_2, such as using nanoparticles to shorten the diffusion lengths,[15,34] incorporating transition-metal cations to catalyze the conversion reactions,[35,36] or increasing the temperature to improve the diffusion rates.[37] Although these approaches improved the kinetics, they have compromised the overall cell performance in other ways, such as resulting in an increased surface area-volume ratio, reduced theoretical energy density, and/or increased PS shuttling (Figure S10).

A Ragone plot of a state-of-the-art intercalation system (NMC 811) and the conversion cathode (FeS_2) data presented here, normalized to the active cathode mass, is presented to broadly highlight the performance differences between the two reaction mechanisms (Figure 4c). The plot suggests intercalation materials are not likely to achieve comparable gravimetric energy to conversion cathodes. Conversely, conversion systems currently cannot match power performance of intercalation materials. This creates a tradeoff: for high energy applications (>1000 Wh/kg), conversion cathodes represent the better choice; but, for higher power applications (>100 W/kg), intercalation systems are currently superior. This compromise becomes more pronounced as conversion cathodes are scaled to higher loadings, on par with intercalation systems (>10mg/cm^2). Our results indicate that while FeS_2 shows promise due to its high theoretical energy density, the current cell design and powder suppliers are not adequate for many commercial applications. Transitioning to smaller particles or incorporating metal catalysts, as mentioned above, provides possible routes to mitigate this tradeoff to achieve both high power and energy densities if their respective limitations are addressed.

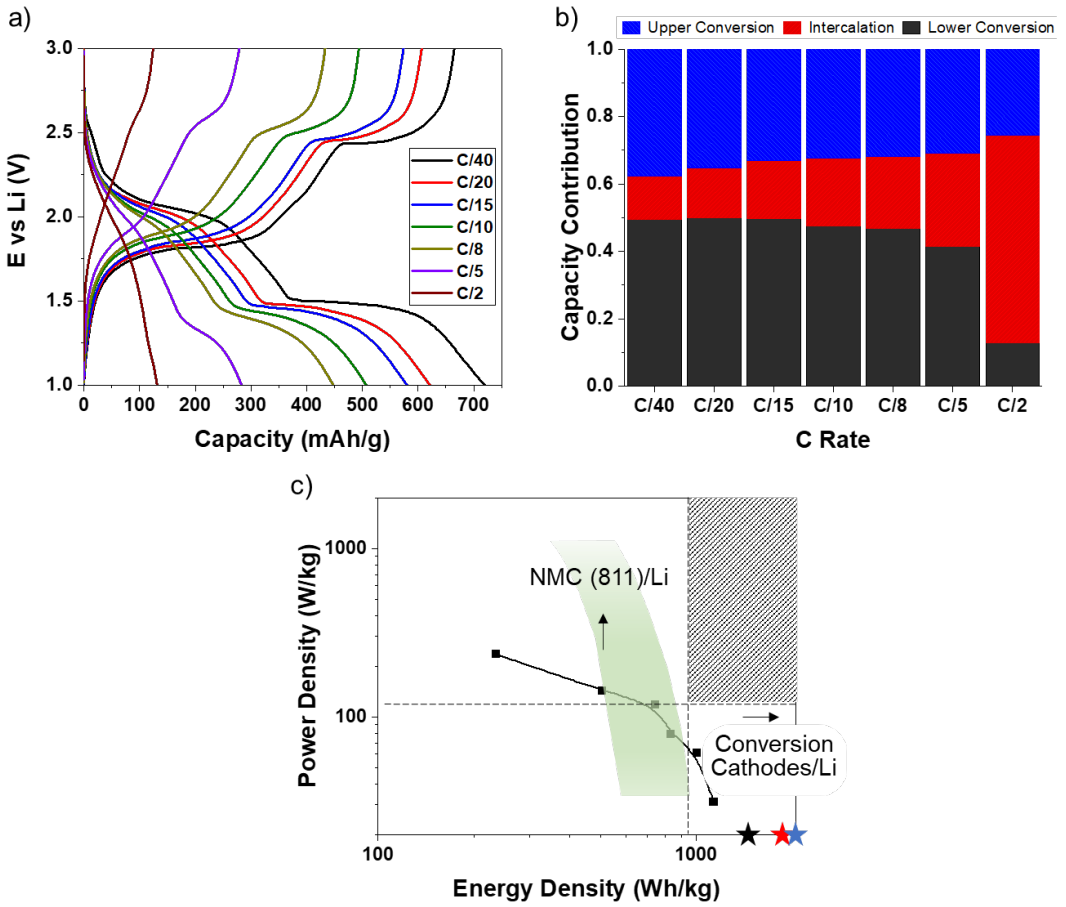

Figure 4: FeS_2 Cycling Kinetics

(a) 2nd galvanostatic cycle at rates varying between C/40-C/2 for a 1.5 mg/cm^2 cell cycled in ILE. (b) Capacity contribution extracted from (A) of the upper conversion, intercalation, and lower conversion reactions cycled at varying C rates as estimated from dQ/dV. (c) Ragone plot (active cathode material) comparing this paper's FeS_2/Li cell (black) to NMC(811)/Li (green shaded) performance in literature.[38–40] Division lines roughly separate the practical regions for intercalation versus conversion systems. The theoretical energy density of FeS_2 (black), FeF_3 (red), and CF_x (blue) is represented as stars.

Understanding the electrochemical limitation and loss mechanisms is key to designing improved conversion cathodes. While FeS_2 is the focus in the present study, we expect that many of our conclusions, such as the benefit of increased pressure and the sluggishness of the conversion reactions, are applicable to other conversion cathode systems, such as FeF_2 and FeF_3. Specifically, our study is first to systematically deconvolute the impact of kinetics and pressure on the reaction mechanisms and their effect on the cycle stability. Contrary to the commonly held assumption that polysulfides are the main loss mechanism, we identify that applied pressure is paramount to counter the adverse effects of matrix and particle degradation associated with large volume changes occurring during (de)lithiation as highlighted by the loss of the electrode electronic conductance. This correlates with the improved performance of solid-state batteries,[12,37] where internal and external pressure compensate for volume-change-induced stresses, while the solid electrolyte suppresses PS shuttling. Furthermore, while PSs are

only relevant to sulfur-bearing conversion cathodes, the relationship between the cathode reaction species and electrolyte on the electrochemical performance should not be ignored for other cathode materials, as seen by the significance of FSI^- to metal fluoride systems.[14] Similarly, understanding the role of kinetics and cell design is key to guiding future modifications of the cell and structure to overcome inherent limitations that might exist in the material. We believe that understanding all three parameters, outlined here for FeS_2, is essential for comprehending and improving current and future conversion cathodes material and cell design limitations.

CONCLUSION

Herein, we deconvolved the contribution of pressure, cathode/electrolyte interaction, and kinetics on the performance of FeS_2/Li cells. We determined that the main capacity loss mechanism stems from the large volume expansion during lithiation. Through improvement of the slurry matrix, such as the mechanical strength and interconnectedness of the conductive matrix or by applying an external pressure to minimize the matrix fracture, the loss from the volume expansion can largely be mitigated. . Sulfur formation in the upper conversion region presents another significant source of capacity loss from polysulfide shuttling, even when mitigation steps that include using low solubility ionic liquid electrolytes are taken. This loss in capacity can be partially mitigated by cycling at higher rates, which limits the polysulfide dissolution. Furthermore, we find that the conversion reactions are kinetically limited, principally from the reduction to metallic iron, hindering the achievable power density for FeS_2/Li cells. Our findings convey that practical use of conversion cathodes, such as FeS_2, require the cells and their inherent materials to be engineered to mitigate volume-expansion-induced pulverization and facilitate rapid-ion diffusion in order to overcome the intrinsic sluggishness of conversion reactions. We expect that improved understanding of the fundamental lithiation mechanism in conversion cathodes will result in better mitigation strategies for future commercialization.

EXPERIMENTAL METHODS:

Electrode Formation:

Commercial FeS_2 powder (Sigma Aldrich, 325 Mesh 99.8%) was ball milled using a Fritsch Pulverisette 7 Premium Line Planetary Micro Mill, a 20 mL stainless steel Fritsch grinding bowl, and 3.0 mm stainless steel Fritsch media. Equivalent mass of FeS_2 (~5 g) and milling media was milled using two iterations at 1000 rpm (3 hrs each), punctuated by a 5-10 minute rest period. The milled material was then separated from the milling media using a mesh. The milled FeS_2 was subsequently stored inside a <1ppm H_2O, Ar glovebox.

Lithium foil (700µm, Sigma Aldrich), reduced graphene oxide (rGO, Graphenea), Super P carbon black (Timcal), polyvinylidene fluoride (PVDF, Kynar HSV900), and n-methyl-2-pyrrolidone (NMP, Sigma Aldrich anhydrous) were used without further processing. The cathode slurries, unless stated, consisted of 75 wt% FeS_2, 7.5 wt% rGO, 7.5 wt% Super P, and 10 wt% PVDF suspended in NMP that were cast onto carbon-coated aluminum foil. Unless stated, all electrodes were fabricated to an approximate loading of 2.5 mg cm^{-2}. All electrodes were dried in a 150°C vacuum oven before assembly. During all steps, exposure to air was kept to a minimum. All electrode loadings and compositions were prepared and deposited through the same process.

Electrochemical Analysis:

1-butyl-1-methylpyrrolidinium bis(trifluoromethylsulfonyl)imide (PYR_{14} TFSI, 99.5%, Solvionic) was first degassed using a vacuum oven before storing inside an Ar-gas-filled glovebox (l ppm H_2O). Lithium bis(fluoromethanesulfonyl)imide (LiFSI, Sigma Aldrich) and Lithium bis(trifluoromethanesulfonyl)imide (LiTFSI, Sigma Aldrich) were used without further processing to prepare 1M LiFSI PYR_{14}TFSI (ILE) and 1M LiTFSI PYR_{14}TFSI electrolytes (TFSI) from the degassed ionic liquid.

FeS_2/Li CR2032 coin cells were galvanostatically cycled using a Biologic SP300 potentiostat with ILE. Pressure was varied inside the cell through compression of a wave spring by stainless steel spacers. Glass fiber separators (Whatman GF/C) were used as separators. The applied current density range ranged from C/40 to C/2 depending on the desired conditions being tested (1C=725 mA/g). Room temperature varied between 21-23ºC. Cycling was performed between 1-3V. Further details are provided in the S.I.

For the conductance measurements, slurries of 75 wt% FeS_2 and 25 wt% PVDF or 95 wt% FeS_2 and 5 wt% PVDF were made through dispersion in NMP. These slurries were dropped onto two 0.25 cm^2 Pt semicircles separated by a 4 μm gap. The cells were cycled in an unpackaged, stacked arrangement against Li metal using the ILE electrolyte and GF/C separator. An applied current of approximately C/20 was used for (de)lithiation.

Physicochemical Analysis:

Scanning electron microscopy (SEM) imaging was performed using a FEI Nova NanoSEM 450 at a 10kV accelerating voltage on FeS_2 electrodes before and after 10 cycles at C/40. Cycled cells were extracted and rinsed with dimethyl carbonate within an Ar glovebox and sealed before loading into the SEM chamber to minimize exposure.

Mechanics Modeling:

The mechanics modeling results were simulated using Sandia's Sierra/Aria Galerkin Finite Element Model code. Three separate regions with different material properties corresponding to FeS_2, $FeS + Li_2S$, and $Fe + 2Li_2S$ were included. The conversion between the different constituents was controlled by level sets with predefined extension velocities. As the reaction progresses, the core of FeS_2 is converted to a shell of $FeS + Li_2S$ which is then converted to a separate shell of $Fe + 2Li_2S$. Volume expansion of the particle was induced through a species expansion stress in the converted shell regions where the arbitrary species dictating the expansion would increase as the level set converts the inner core material. The solid stresses and displacements within the particle were evaluated using a Lagrangian approach and external pressure was applied through a boundary condition on the outermost surface of the particle.

ASSOCIATED CONTENT

Supporting Information:

Cell fabrication process, Mechanical stress snapshot, SEM imaging of cycled electrodes, Capacity contribution with relationship to pressure, dQ/dV, TFSI electrochemical cycling, Extended cycling, Cell stability after aging, Particle size distribution, Cycle stability with temperature

AUTHOR INFORMATION

dsashby@sandia.gov, aatalin@sandia.gov

The authors declare no competing financial interest.

ACKNOWLEDGMENT

The work at Sandia National Laboratories was supported by the Laboratory-Directed Research and Development (LDRD) Programs. Sandia National Laboratories is a multimission laboratory managed and operated by National Technology and Engineering Solutions of Sandia, LLC, a wholly owned subsidiary of Honeywell International Inc., for the U.S. Department of Energy's National Nuclear Security Administration under contract DE-NA-0003525. This paper describes objective technical results and analysis. Any subjective views or opinions that might be expressed in the paper do not necessarily represent the views of the U.S. Department of Energy or the United States Government. The authors further acknowledge Brian Werner of Sandia National Laboratories for determining the pressure associated with the spring compression.

REFERENCES

(1) Hannan, M. A.; Hoque, M. M.; Mohamed, A.; Ayob, A. Review of Energy Storage Systems for Electric Vehicle Applications: Issues and Challenges. *Renew. Sustain. Energy Rev.* **2017**, *69*, 771–789.

(2) Baumann, M.; Weil, M.; Peters, J. F.; Chibeles-Martins, N.; Moniz, A. B. A Review of Multi-Criteria Decision Making Approaches for Evaluating Energy Storage Systems for Grid Applications. *Renew. Sustain. Energy Rev.* **2019**, *107*, 516–534.

(3) Feng, K.; Li, M.; Liu, W.; Kashkooli, A. G.; Xiao, X.; Cai, M.; Chen, Z. Silicon-Based Anodes for Lithium-Ion Batteries: From Fundamentals to Practical Applications. *Small* **2018**, *14* (8), 1702737.

(4) Li, H.; Yamaguchi, T.; Matsumoto, S.; Hoshikawa, H.; Kumagai, T.; Okamoto, N. L.; Ichitsubo, T. Circumventing Huge Volume Strain in Alloy Anodes of Lithium Batteries. *Nat. Commun. 2020 111* **2020**, *11* (1), 1–8.

(5) Jia, R.; Yue, J.; Xia, Q.; Xu, J.; Zhu, X.; Sun, S.; Zhai, T.; Xia, H. Carbon Shelled Porous SnO2-δ Nanosheet Arrays as Advanced Anodes for Lithium-Ion Batteries. *Energy Storage Mater.* **2018**, *13* (February), 303–311.

(6) Wu, F.; Yushin, G. Conversion Cathodes for Rechargeable Lithium and Lithium-Ion Batteries. *Energy Environ. Sci.* **2017**, *10* (2), 435–459.

(7) Yu, S.-H.; Feng, X.; Zhang, N.; Seok, J.; Abruña, H. D. Understanding Conversion-Type Electrodes for Lithium Rechargeable Batteries. *Acc. Chem. Res.* **2018**, *51* (2), 273–281.

(8) Hua, X.; Eggeman, A. S.; Castillo-Martínez, E.; Robert, R.; Geddes, H. S.; Lu, Z.; Pickard, C. J.; Meng, W.; Wiaderek, K. M.; Pereira, N.; et al. Revisiting Metal Fluorides as Lithium-Ion Battery Cathodes. *Nat. Mater.* **2021**, *20* (6), 841–850.

(9) Zhu, Y.; Fan, X.; Suo, L.; Luo, C.; Gao, T.; Wang, C. Electrospun FeS2 @Carbon Fiber Electrode as a High Energy Density Cathode for Rechargeable Lithium Batteries. *ACS Nano* **2016**, *10*, 1529–1538.

(10) Choi, J. W.; Aurbach, D. Promise and Reality of Post-Lithium-Ion Batteries with High Energy Densities. *Nat. Rev. Mater.* **2016**, *1* (4), 16013.

(11) Zhang, S. S.; Tran, D. T. Mechanism and Solution for the Capacity Fading of Li/FeS2 Battery. *J. Electrochem. Soc.* **2016**, *163* (5), A792–A797.

(12) Pelé, V.; Flamary, F.; Bourgeois, L.; Pecquenard, B.; Le Cras, F. Perfect Reversibility of the Lithium Insertion in FeS2: The Combined Effects of All-Solid-State and Thin Film Cell Configurations. *Electrochem. commun.* **2015**, *51*, 81–84.

(13) Zou, J.; Zhao, J.; Wang, B.; Chen, S.; Chen, P.; Ran, Q.; Li, L.; Wang, X.; Yao, J.; Li, H.; et al. Unraveling the Reaction Mechanism of FeS2 as a Li-Ion Battery Cathode. *ACS Appl. Mater. Interfaces* **2020**, *12* (40), 44850–44857.

(14) Xiao, A. W.; Lee, H. J.; Capone, I.; Robertson, A.; Wi, T.-U.; Fawdon, J.; Wheeler, S.; Lee, H.-W.; Grobert, N.; Pasta, M. Understanding the Conversion Mechanism and Performance of Monodisperse FeF2 Nanocrystal Cathodes. *Nat. Mater.* **2020**, *19* (6), 644–654.

(15) Douglas, A.; Carter, R.; Oakes, L.; Share, K.; Cohn, A. P.; Pint, C. L. Ultrafine Iron Pyrite (FeS2) Nanocrystals Improve Sodium-Sulfur and Lithium-Sulfur Conversion Reactions for Efficient Batteries. *ACS Nano* **2015**, *9* (11), 11156–11165.

(16) Energizer. *Lithium Iron Disulfide-Li/FeS2 Application Manual*; 2004.

(17) Boebinger, M. G.; Yeh, D.; Xu, M.; Xia, S.; Zhu, T.; Mcdowell, M. T.; Miles, B. C.; Wang, B.; Papakyriakou, M.; Lewis, J. A.; et al. Avoiding Fracture in a Conversion Battery Material through Reaction with Larger Ions. *Joule* **2018**, *2*, 1783–1799.

(18) Xu, X.; Cai, T.; Meng, Z.; Ying, H.; Xie, Y.; Zhu, X.; Han, W. Q. FeS2 Nanocrystals Prepared in Hierarchical Porous Carbon for Lithium-Ion Battery. *J. Power Sources* **2016**, *331*, 366–372.

(19) Yang, K.; Guo, Q.; Li, H.; Hao, X.; Ma, Y.; Yang, M.; Zhai, T.; Savilov, S. V.; Lunin, V. V.; Xia, H. Highly Efficient Sol-Gel Synthesis for ZnS@N, S Co-Doped Carbon Nanosheets with Embedded Heterostructure for Sodium Ion Batteries. *J. Power Sources* **2018**, *402* (July), 340–344.

(20) Zhao, X.; Lehto, V.-P. Challenges and Prospects of Nanosized Silicon Anodes in Lithium-Ion Batteries. *Nanotechnology* **2020**, *32* (4), 042002.

(21) Song, X.; Tian, D.; Qiu, Y.; Sun, X.; Jiang, B.; Zhao, C.; Zhang, Y.; Fan, L.; Zhang, N. Improving Poisoning Resistance of Electrocatalysts via Alloying Strategy for High-Performance Lithium-Sulfur Batteries. *Energy Storage Mater.* **2021**, *41* (February), 248–254.

(22) Evans, T.; Piper, D. M.; Kim, S. C.; Han, S. S.; Bhat, V.; Oh, K. H.; Lee, S.-H. Ionic Liquid Enabled FeS_2 for High-Energy-Density Lithium-Ion Batteries. *Adv. Mater.* **2014**, *26* (43), 7386–7392.

(23) Smith, L. C.; Malati, P.; Fang, J.; Richardson, W.; Ashby, D.; Lai, C.-H.; Dunn, B. S. Sol–Gel Encapsulated Lithium Polysulfide Catholyte and Its Application in Lithium–Sulfur Batteries. *Mater.*

Horiz. **2016**, *3* (2), 137–144.

(24) Shi, Z.; Li, M.; Sun, J.; Chen, Z. Defect Engineering for Expediting Li–S Chemistry: Strategies, Mechanisms, and Perspectives. *Adv. Energy Mater.* **2021**, *11* (23).

(25) Xu, X.; Liu, J.; Liu, Z.; Shen, J.; Hu, R.; Liu, J.; Ouyang, L.; Zhang, L.; Zhu, M. Robust Pitaya-Structured Pyrite as High Energy Density Cathode for High-Rate Lithium Batteries. *ACS Nano* **2017**, *11* (9), 9033–9040.

(26) Li, C.; Ward, A. L.; Doris, S. E.; Pascal, T. A.; Prendergast, D.; Helms, B. A. Polysulfide-Blocking Microporous Polymer Membrane Tailored for Hybrid Li-Sulfur Flow Batteries. *Nano Lett.* **2015**, *15* (9), 5724–5729.

(27) Schorr, B. N. B.; Kolesnichenko, I. V.; Merrill, L. C.; Wygant, B. R.; Harrison, K. L.; Lambert, T. N. Stable Cycling of Lithium Batteries Utilizing Iron Disulfide Nanoparticles. *ACS Appl. Nano Mater.* **2021**, *4* (11), 11636–11643.

(28) Horner, J. S.; Whang, G.; Ashby, D. S.; Kolesnichenko, I. V.; Lambert, T. N.; Dunn, B. S.; Talin, A. A.; Roberts, S. A. Electrochemical Modeling of GITT Measurements for Improved Solid-State Diffusion Coefficient Evaluation. *ACS Appl. Energy Mater.* **2021**.

(29) Xu, L.; Hu, Y.; Zhang, H.; Jiang, H.; Li, C. Confined Synthesis of FeS2 Nanoparticles Encapsulated in Carbon Nanotube Hybrids for Ultrastable Lithium-Ion Batteries. *ACS Sustain. Chem. Eng.* **2016**, *4* (8), 4251–4255.

(30) Ong, S. P.; Andreussi, O.; Wu, Y.; Marzari, N. Electrochemical Windows of Room-Temperature Ionic Liquids from Molecular Dynamics and Density Functional Theory Calculations. *Chem. Mater.* **2011**, *23*, 2979–2986.

(31) De Jong, M.; Chen, W.; Angsten, T.; Jain, A.; Notestine, R.; Gamst, A.; Sluiter, M.; Ande, C. K.; Van Der Zwaag, S.; Plata, J. J.; et al. Charting the Complete Elastic Properties of Inorganic Crystalline Compounds. *Sci. Data* **2015**, *2* (1), 1–13.

(32) Busche, M. R.; Adelhelm, P.; Sommer, H.; Schneider, H.; Leitner, K.; Janek, J. Systematical Electrochemical Study on the Parasitic Shuttle-Effect in Lithium-Sulfur-Cells at Different Temperatures and Different Rates. *J. Power Sources* **2014**, *259*, 289–299.

(33) Park, J.-W.; Ueno, K.; Tachikawa, N.; Dokko, K.; Watanabe, M. Ionic Liquid Electrolytes for Lithium–Sulfur Batteries. *J. Phys. Chem. C* **2013**, *117* (40), 20531–20541.

(34) Liu, W. L.; Rui, X. H.; Tan, H. T.; Xu, C.; Yan, Q. Y.; Hng, H. H. Solvothermal Synthesis of Pyrite FeS2 Nanocubes and Their Superior High Rate Lithium Storage Properties. *RSC Adv.* **2014**, *4* (90), 48770–48776.

(35) Wan, H.; Liu, G.; Li, Y.; Weng, W.; Mwizerwa, J. P.; Tian, Z.; Chen, L.; Yao, X. Transitional Metal Catalytic Pyrite Cathode Enables Ultrastable Four-Electron-Based All-Solid-State Lithium Batteries. *ACS Nano* **2019**, *13* (8), 9551–9560.

(36) Zhong, M. e.; Guan, J.; Feng, Q.; Wu, X.; Xiao, Z.; Zhang, W.; Tong, S.; Zhou, N.; Gong, D. Accelerated Polysulfide Redox Kinetics Revealed by Ternary Sandwich-Type S@Co/N-Doped Carbon Nanosheet for High-Performance Lithium-Sulfur Batteries. *Carbon N. Y.* **2018**, *128*, 86–96.

(37) Yersak, T. A.; Macpherson, H. A.; Kim, S. C.; Le, V. D.; Kang, C. S.; Son, S. B.; Kim, Y. H.; Trevey, J. E.; Oh, K. H.; Stol dt, C.; et al. Solid State Enabled Reversible Four Electron Storage. *Adv. Energy Mater.* **2013**, *3* (1), 120–127.

(38) Sun, H.; Zhu, G.; Zhu, Y.; Lin, M.-C.; Chen, H.; Li, Y.-Y.; Hung, W. H.; Zhou, B.; Wang, X.; Bai, Y.; et al. High-Safety and High-Energy-Density Lithium Metal Batteries in a Novel Ionic-Liquid Electrolyte. *Adv. Mater.* **2020**, *32* (26), 2001741.

(39) Xue, W.; Huang, M.; Li, Y.; Guang Zhu, Y.; Gao, R.; Xiao, X.; Zhang, W.; Li, S.; Xu, G.; Yu, Y.; et al. Ultra-High-Voltage Ni-Rich Layered Cathodes in Practical Li Metal Batteries Enabled by a Sulfonamide-Based Electrolyte. *Nat. Energy* **2021**, *6*, 495–505.

(40) Schmidt, D.; Kamlah, M.; Knoblauch, V. Highly Densified NCM-Cathodes for High Energy Li-Ion Batteries: Microstructural Evolution during Densification and Its Influence on the Performance of the Electrodes. *J. Energy Storage* **2018**, *17*, 213–223.

Understanding the Electrochemical Performance of Li^+ Conversion Cathodes

David S. Ashby[1,], Jeff Horner[2], Grace Whang[3], Aliya Lapp[1], Scott Roberts[2], Bruce Dunn[3],Igor Kolesnichenko[2], Timothy Lambert[2], and A. Alec Talin[1,*]*

[1]Sandia National Laboratories, Livermore, California 94550, USA.

[2]Sandia National Laboratories, Albuquerque, New Mexico, 87116, USA

[3]Department of Materials Science and Engineering, University of California, Los Angeles, CA 90095, USA.

Corresponding Authors*

Supplemental:

Cell fabrication process:

Application of pressure to the FeS_2 cells was controlled through compression of an internal wave spring whose load-displacement curve is known. The applied load (~50 N) was calculated from the expected spring compression assumed from the thickness of the cell components (steel spacers, spring, Li metal, separator, and cathode) and the CR2032 free volume. The load was normalized to the electrode area (1.6 cm^2). An assumed permanent compression of the Li metal and separator from the addition of extra spacers was estimated when calculating the spring compression, introducing inherent error in our calculated pressures. For the zero-pressure cell, the quantity of spacers was controlled to ensure minimal compression of the spring.

When manufacturing the ionogel cell, the quantity of spacers was controlled to ensure minimal compression of the spring, mimicking the zero-pressure, liquid cell. All internal pressure corresponds to the rigidity provided by the silica matrix. The modulus was calculated previously from nanoindentation tests.

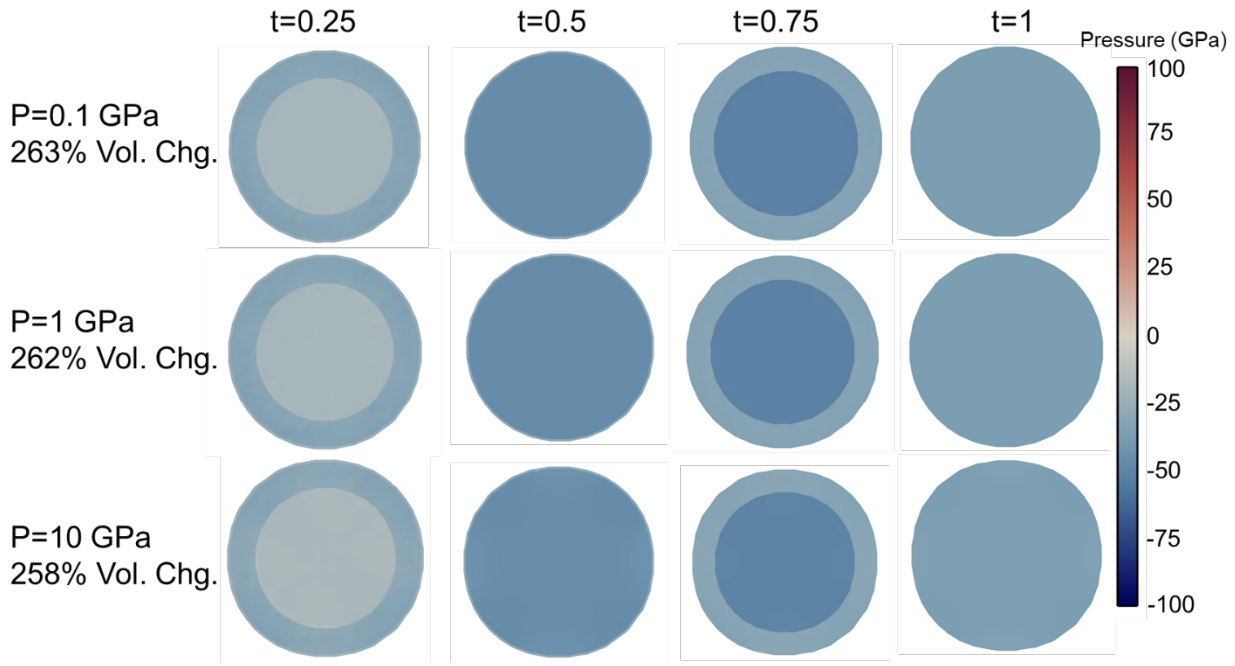

Figure S1: Particle Stress Fields

Internal mechanical stress snapshots after incorporation of approximately 1 (t=0.25), 2 (t=0.5), 3 (t=0.75), and 4 (t=1) moles Li^+ generated during arbitrarily sized, FeS_2 single particle volume expansion. The particles were 3-axial, point constrained at varying external pressures. Compression is considered positive for the simulation. The average pressures were extracted and plotted in Figure 1D.

As the first lithiation progresses, a core-shell structure materializes with a shell and core under varying degrees of tension, dependent on the state of lithiation. Tension exists in both the shell and core due to the shell expansion, which during conversion pulls the core outward increasing its volume. With values above the modulus of the Li_2S, cracking is expected to occur throughout the lithiation process.

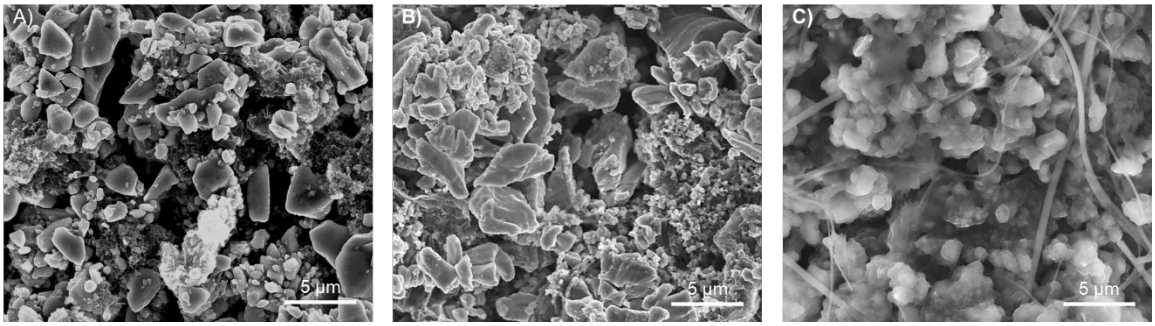

Figure S2: SEM Imaging of FeS_2 Cathodes

A) Uncycled electrode with a composition of 80 wt% FeS_2 at 2.5 mg/cm^2. B) Cycled electrode with a composition of 80 wt% FeS_2 at 2.5 mg/cm^2 under ~300 kPa (Figure 1). C) Cycled electrode with a composition of 80 wt% FeS_2 at 2.5 mg/cm^2 under ~0 kPa (Figure 1).

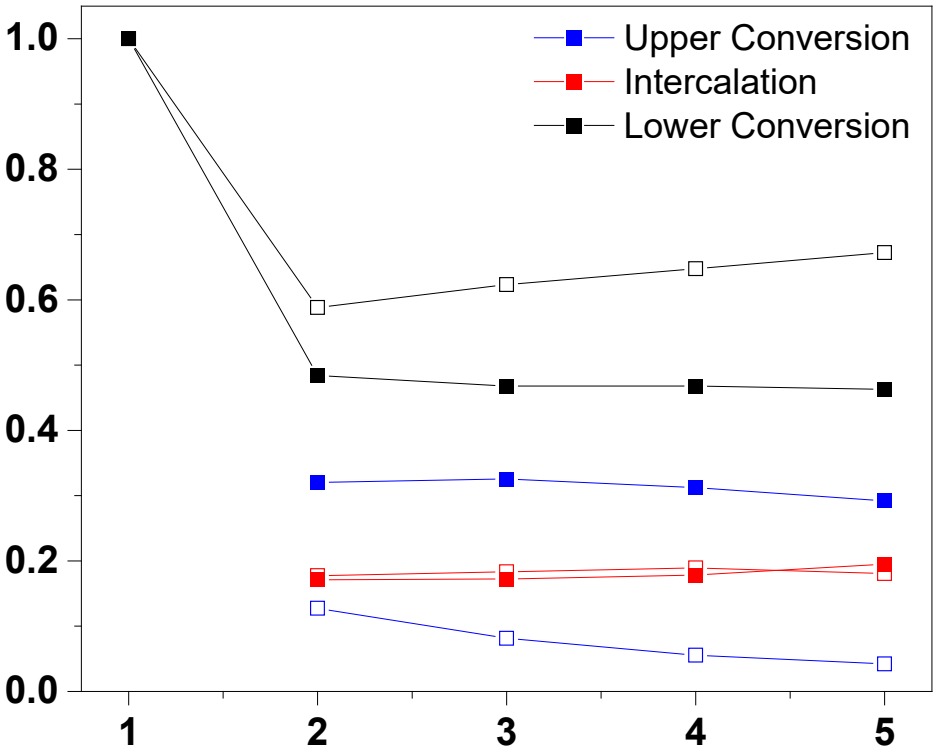

Figure S3: Capacity Contribution Relationship to Pressure

Capacity contribution during discharge of the upper conversion (>~1.9V), intercalation, and lower conversion (~<1.5V) reactions for the 80 wt% FeS_2 1 mg/cm^2 cells under ~300 kPa (solid) and under no pressure (open) in figure 1B. The upper conversion contribution is found to decrease with each cycle while the lower conversion increases when not under pressure as more material is loss to increased polysulfide dissolution from particle pulverization. Stable contributions are identified for the cell under pressure over the first 5 cycles.

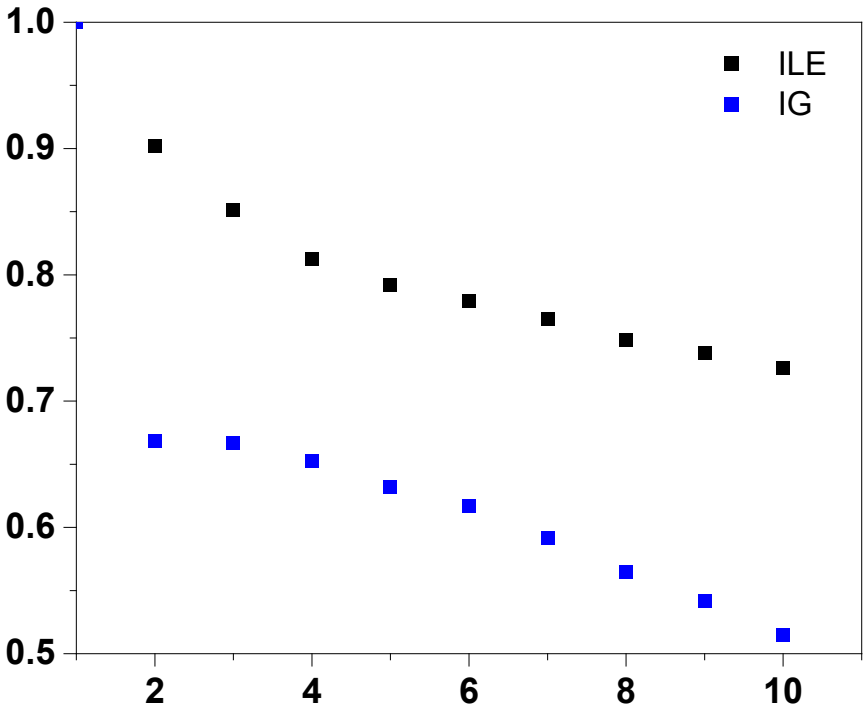

Figure S4: Electrochemical Stability with an Ionogel Solid Electrolyte

Electrochemical performance of FeS_2/Li cells cycled at C/40 using an ionogel (IG, blue) or ionic liquid electrolyte (ILE, black). Ionogel was used to mimic the external pressure applied to the ILE cell in Figure 1B. Similar cycle low cycle losses are found between cycles 2-10 for the IG (1.7%/cycle) and ILE (2.0%/cycle). The lower overall capacity of the ionogel system can be attributed to the lower ionic conductivity that the base liquid.

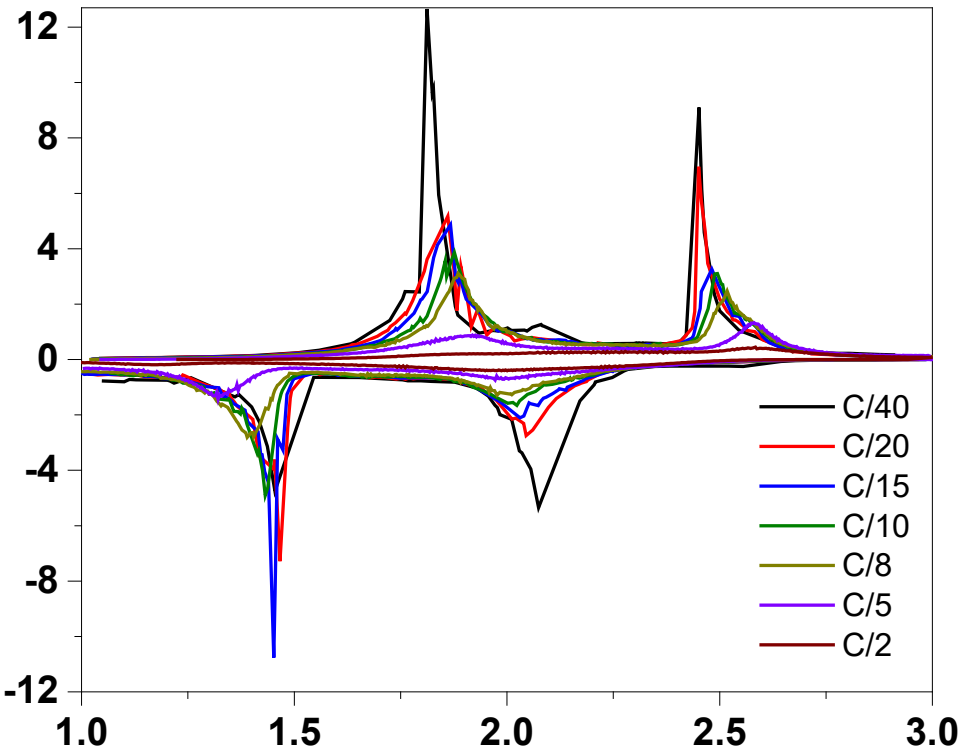

Figure S5: dQ/dV of FeS_2 with Current Density

dQ/dV extracted from the rate capability study in Figure 3A used to differentiate the upper conversion, intercalation, and lower conversion regions. As the rate increases, the (de)lithiation reactions become increasingly polarized and broadens over a wider voltage.

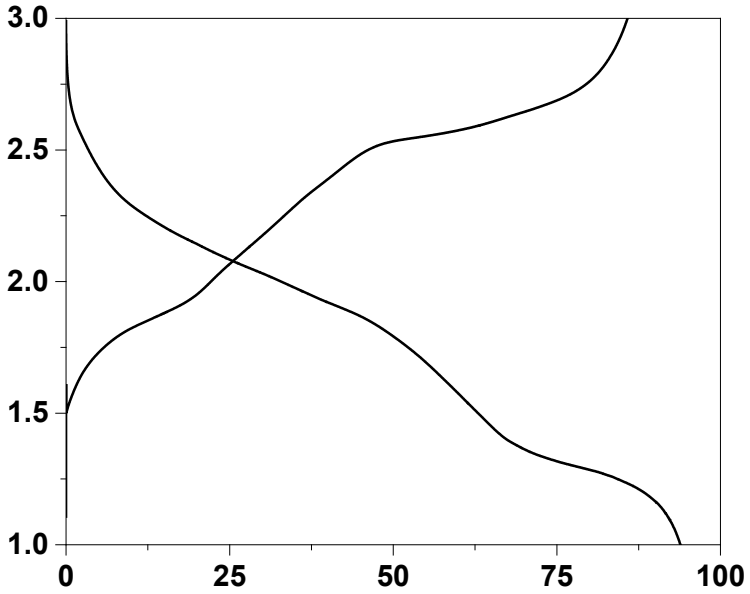

Figure S6: FeS_2/Li Cycling in 1M LiTFSI $PYR_{14}TFSI$

2nd galvanostatic cycle of a FeS_2/Li metal cell with 1M LiTFSI $PYR_{14}TFSI$ electrolyte cycled at C/20. The higher viscosity and lower ionic conductivity of the TFSI electrolyte led to significantly lower capacities than the LiFSI system (Figure 2D) even with the lower polysulfide solubility of the TFSI system[31].

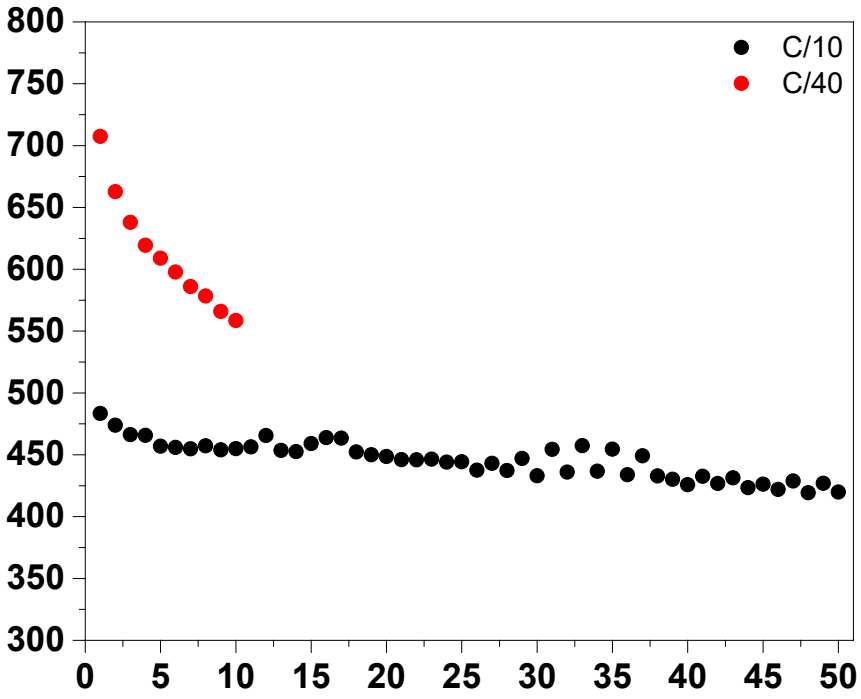

Figure S7: Extended Electrochemical Performance of FeS_2

Extended electrochemical performance of FeS_2/Li cells cycled at C/10 for 50 cycles (Figure 2D). As comparison, 10 cycles at C/40 (red) is included. By decreasing the current, the cycle becomes stable over 50 cycles (0.9 mAh/g loss per cycle) at the expense of a lower capacity (~60%).

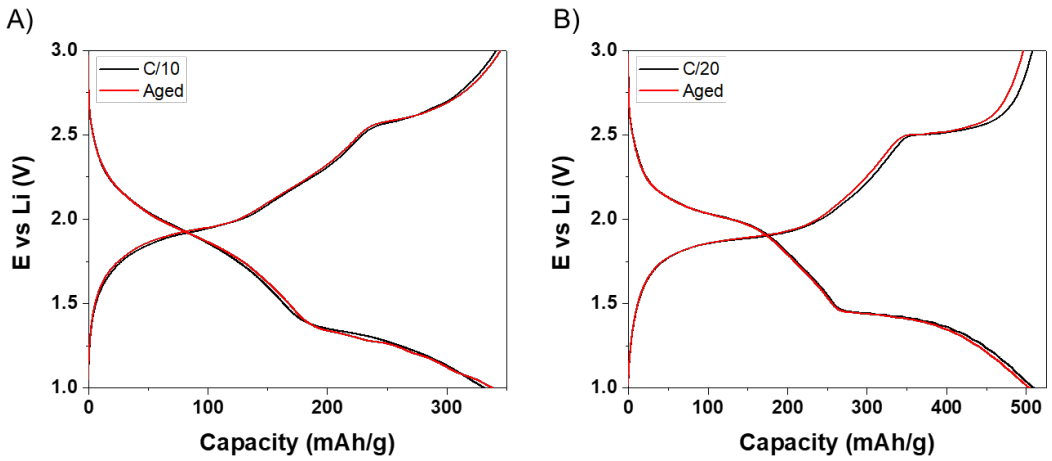

Figure S8: Cycle Stability after Rest

Galvanostatic cycling of C/10 (A) and C/20 (B) cells shown in Figure 2D. The cells were delithiated to after or before sulfur formation, 3V (A) or 2V (B) respectively, before being allowed to rest at OCV for 10 days. After resting, the cells were recycled at the same currents for two cycles to determine the stability. As seen, neither cell loss capacity after resting even though (A) was stopped with sulfur as a final product.

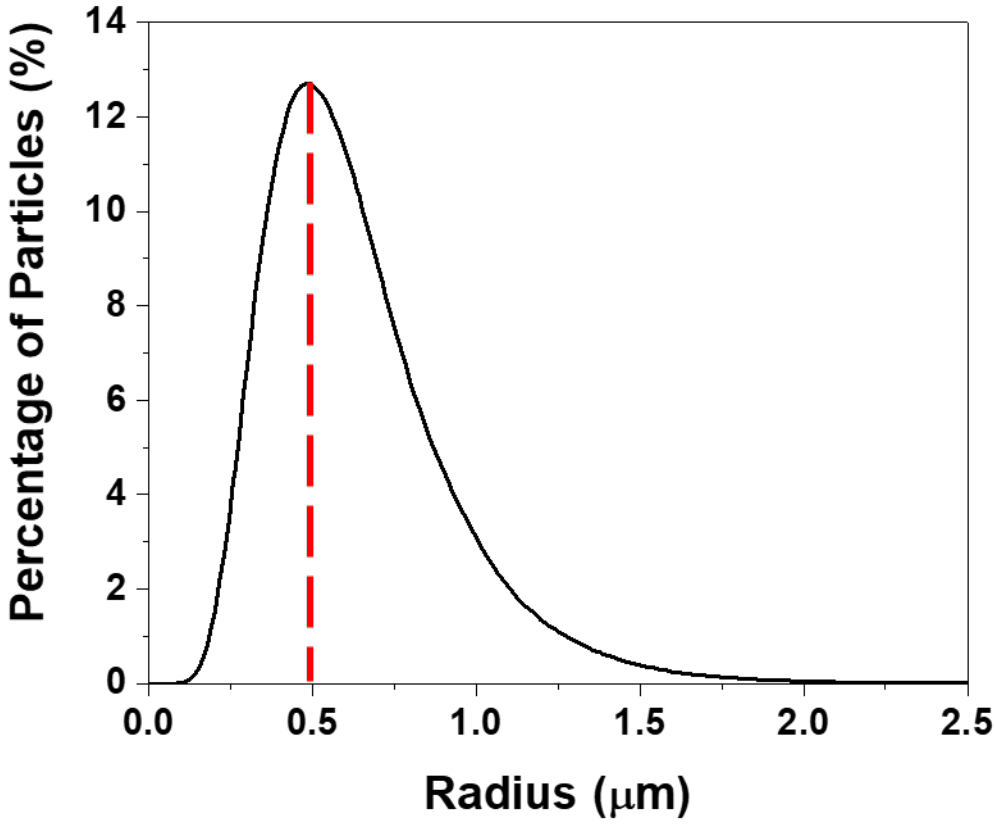

Figure S9: Particle Size Distribution of FeS_2

Particle size distribution of the FeS_2 used in this study. The particle ranged in radius from 200nm to 2μm with an average radius of 0.5μm. Reducing the particle size to the nanoscale would improve the kinetics by effectively increasing the total accessible particle volume at higher current densities.

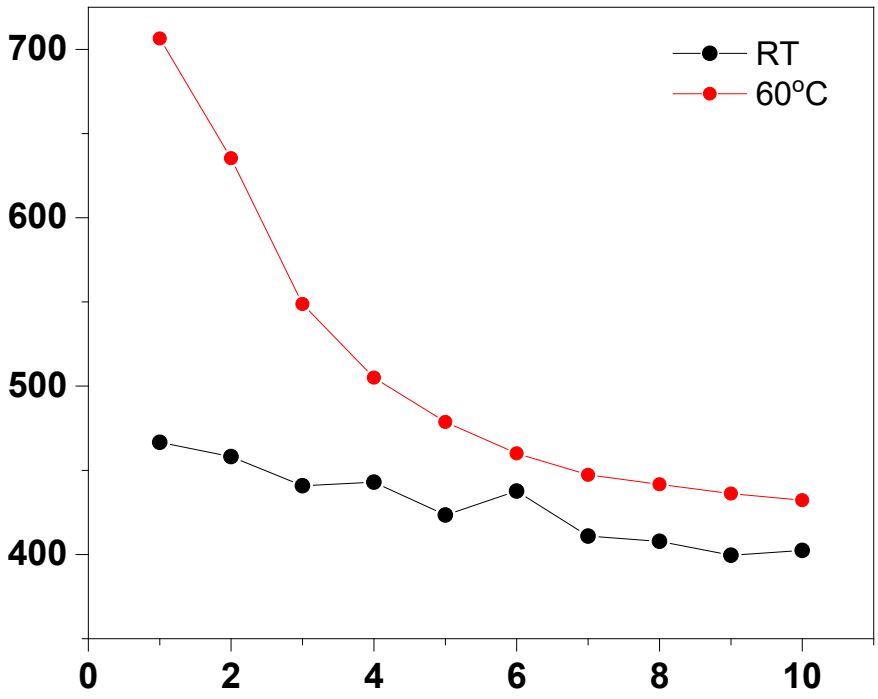

Figure S10:Thermal Influence on the FeS_2 Performance

Electrochemical performance of FeS_2/Li cells cycled at C/10 at room temperature (black, Figure 2D) and 60°C (red). While a higher capacity is obtained by elevating the operating temperature, the increased temperature increased the polysulfide solubility leading to an exacerbated capacity loss per cycle.